Available online at www.sciencedirect.com
ScienceDirect
PHOTONICS AND NANOSTRUCTURES
Fundamentals and Applications
Photonics and Nanostructures – Fundamentals and Applications 6 (2008) 213–218
www.elsevier.com/locate/photonics

Accurate determination of the functional hole size in photonic crystal slabs using optical methods

Daryl M. Beggs *, Liam O'Faolain, Thomas F. Krauss

School of Physics and Astronomy, University of St Andrews, St Andrews, Fife KY16 9SS, UK

Received 25 June 2008; received in revised form 25 September 2008; accepted 26 September 2008
Available online 14 October 2008

Abstract

Control and repeatability in the fabrication of two-dimensional photonic crystal (PhC) slabs is becoming increasingly important as the technology matures towards practical applications. A key problem in this respect is the determination of the actual hole size in finished devices. We have developed an optical method for measuring the hole size in PhC slabs as an alternative to the inspection of scanning electron microscope (SEM) images. The optical method relies on determining the cut-off frequency of W1 PhC waveguides, which is easily measured and compared to calculations as a function of hole size. We show that the typical error in the measurement of hole diameter is approximately 2%, or 5 nm. This level of accuracy is a significant improvement over current methods, which rely on the inspection by SEM. SEM inspection can introduce large systematic errors because different electron detectors, and even different settings of the same detector, will provide differing contrasts between a hole and its edge. Such errors can be of the order of 20 nm, or as much as 5–10% of the absolute hole diameter. Furthermore, our method provides the *functional* or *effective* hole size, which determines the photonic function of the device, and which may be different from the *physical* hole size.
© 2008 Elsevier B.V. All rights reserved.

PACS : 42.70.Qs; 42.82.Cr

Keywords: Control; Repeatability; Photonic crystal slab; W1 waveguides

Two-dimensional slab photonic crystals (PhCs) have been the subject of intensive research over the last decade. They can be made by applying the mature planar lithographic patterning and etching technology developed by the semiconductor industry [1]. In this framework, an especially important material is silicon-on-insulator (SOI) – a thin (~200 nm) layer of silicon on a thicker (~2 μm) silica substrate – which offers the opportunity of true opto-electronic monolithic integration.

Recently, control and repeatability in fabrication are becoming increasingly important issues as photonic crystal slab technology matures into real device applications [2–7]. All the PhC designs – from those using superprism effects, to high-Q nanocavities, to optimised waveguides and bends, to filters and switches – rely on accurately controlling the sizes of the air holes that constitute the photonic crystal [8–16]. Indeed, many designs have several distinct hole sizes, and in these cases, the relative (as well as the absolute) sizes of the holes are important for optimised device performance. Even where the absolute performance (i.e. independent from operating wavelength) of a device is tolerant to the final hole size in the device, the operating wavelength is critically dependent on this size, a fact that is often conveniently overlooked in the literature. For example, a small error in the hole size of just a few nm can mean a shift of tens of nm in the operating

* Corresponding author. Tel.: +44 1334 467336.
E-mail addresses: daryl.beggs@st-andrews.ac.uk, daryl.beggs@dunelm.org.uk (D.M. Beggs).

1569-4410/$ – see front matter © 2008 Elsevier B.V. All rights reserved.
doi:10.1016/j.photonics.2008.09.003

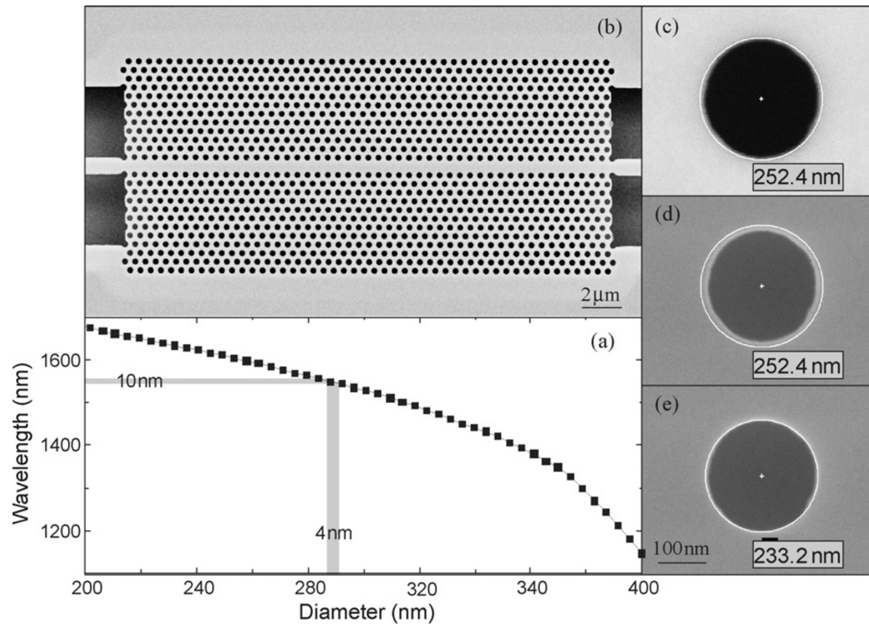

Fig. 1. (a) Graph of operating wavelength against diameter of holes for a typical photonic crystal device. The horizontal and vertical grey bars illustrate the level of control required over the size to achieve an operation within a 10 nm window around 1550 nm. (b) SEM of a membrane W1 photonic crystal waveguide. The waveguide shown is typical of the devices prepared for this paper—it has a length of 48*a* and photonic wires are used for the coupling of light to the optical facets. (c–e) SEM images of the same hole in the silicon slab, taken at identical magnifications (100,000×), but with two different detector settings. The diameter of the white circle is indicated in each case; (d) is the same image as (e) but has the same circle as (c).

wavelength of the device, which is significant given that typical bandwidths for photonic crystal devices are of the order of nanometres. Fig. 1(a) illustrates the problem: it shows the calculated operating wavelength of a photonic crystal waveguide as the hole size in the device is altered. As indicated by the grey bars, the requirement for achieving a device operating in a 10 nm wavelength window around 1550 nm is that the hole diameters are controlled to within 4 nm. Using typical lithographic patterning methods, accurate control of the hole size to this level is very difficult and needs to be carefully controlled.

A related problem is the measurement and determination of the hole sizes in the finished devices. Typical methods rely on the inspection of scanning electron microscope (SEM) images, which introduces both a random error that arises from the measurement of a considerable number of holes, as well as a large systematic error. Different electron detectors, and even different parameter sets of the same detector, provide differing contrasts between the hole and its edge, leading to different apparent hole sizes in the images. Fig. 1(c–e), which shows SEM images of the same hole with two different detector set-ups, illustrates the problem. Such errors can be of the order of 20 nm, which can be as much as 10% of the hole diameter for photonic crystals operating in the near-infrared with a typical hole diameter of 200–300 nm. Furthermore, the physical hole size may be different from the hole size that determines the optical response of the structure, because there may be a variation of hole size across the sample, the hole shape may differ from that of an ideal cylinder, or (this is especially true for GaAs samples [17]) an oxide skin may form on the inside of the hole. So even if the true physical value of each hole was known, it would not necessarily yield the information required to determine the photonic function of the device.

This paper describes an accurate optical method for measuring the *average* effective hole size of two-dimensional PhC slabs as an alternative to SEM inspection of *individual* holes. The optical method relies on the well-studied W1 PhC waveguide [18–21]—a defect waveguide of one row of missing holes in an hexagonal lattice of holes, an example of which is shown in Fig. 1(b). By patterning and fabricating reference W1 waveguides (with the same size holes as the device in question) on-chip, the cut-off frequency of the waveguiding defect state can be measured and compared to calculations of this frequency as a function of the hole size.

The hole size dependence of another spectral feature (the W3 mini-stop-band) was previously used to

determine the accuracy of the proximity-effect-correction [7]. In this paper, we use the W1 cut-off frequency to measure the size of the fabricated holes. The W1 cut-off frequency has previously been shown to be very sensitive to changes in hole size [7], making it an ideal spectral feature to use in this measurement. However, the (well documented) problems of coupling to the slow-light mode and identifying the cut-off from transmission measurements must be addressed. In this paper, we chose to do this by including a suitable error in the measurement of the cut-off. Via an analysis of this and the other sources of error, the problems mentioned can be subsumed into the error bar of the measurement of the hole diameter.

As an example, we have fabricated several W1 PhC waveguide designs by patterning a resist with electron-beam lithography on an SOI wafer. The fabrication of the W1 waveguides was repeated for several different electron-beam doses, and optical measurements show the enlargement of the holes as a function of the base dose. These experimental observations are compared to numerical calculations in order to determine the hole diameters accurately via the measured cut-off wavelength. Then, by analysing the sources of error in the measurement, we show that the typical error is approximately 2%, or just 5 nm for operation around 1.5 μm wavelength. This error is a significant improvement over the SEM inspection method.

1. Calculations and measurements

The functional dependence of the W1 dispersion relation is well known. An example is shown in the inset of Fig. 2: the important feature for the present discussion is the slow-light region (where the magnitude of the group velocity is small) and the cut-off frequency (ν_0) just below the fundamental mode of the PhC waveguide. At frequencies above the cut-off, light is guided by the PhC waveguide, and the transmission is high, whereas below this cut-off, there are no guided modes and the transmission is very low. Hence this cut-off is easily measured in simple transmission experiments.

The calculation of the cut-off frequency is also straightforward. The simplest method is to calculate the bandstructure using a three-dimensional (3D) plane-wave method [22], and we have used the freely available MPB package [23]. The 3D slab structure adds a fundamental length to the structure – the slab height h – which does not scale with the lattice constant a. This means that the calculations must be performed for each value of a considered. The calculational grid that we used has a dimension of $a/16$ within the plane of the slab, and $a/30$ out of the plane to ensure convergence of the eigenvalues to better than 0.1%. A refractive index of 3.48 was used for the silicon slab [24]. Fig. 2 shows the calculated cut-off frequency as a function of the hole diameter for the membrane geometry.

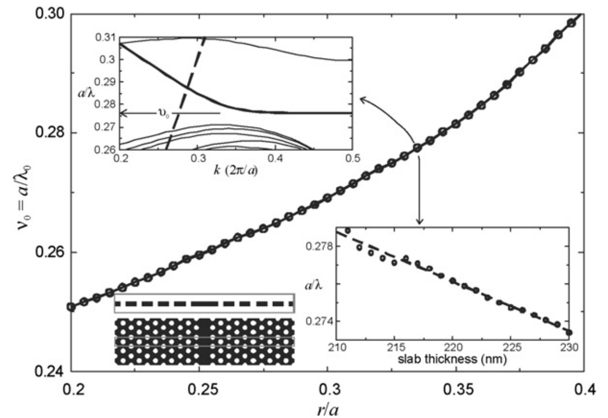

Fig. 2. Calculations of the cut-off frequency of the W1 waveguiding defect state as a function of the hole radius for the membrane geometry ($a = 430$ nm, $h = 220$ nm). Inset – top left – the bandstructure as calculated for the indicated radius of holes (0.33a). The bold line highlights the waveguiding defect state of the W1, and the dashed line indicates the position of the lightline of the cladding. Inset – bottom right – the calculated cut-off frequency as a function of the silicon slab thickness for the indicated radius (0.33a).

For the fabrication, a 350 nm thick layer of ZEP-520A was deposited on SOI wafers supplied by SOITEC (220 ± 5 nm thick Si layer with 2 μm SiO_2 buffer) to act as an etch mask and resist. The patterns were generated by electron-beam lithography, and transferred directly into the silicon layer using low power, low DC-bias reactive ion etching with a SF_6/CHF_3 gas mix—a process known to yield very low-loss photonic crystal waveguides [25]. After the dry etching step, the SiO_2 buffer is selectively removed by etching in a HF solution to form an airbridge in the region of the PhC waveguides (the access waveguides are protected by a photoresist). Fig. 1(b) shows an example of a fabricated device.

Following fabrication, the cut-off wavelengths of the W1 defect guiding state are measured in an end-fire set-up, using a broad-band (1480–1680 nm) LED source and an optical spectrum analyser (Advantest Q8384). Fig. 3 shows the measured transmission spectra of three different devices patterned using different electron-beam doses.

2. Analysis of errors

The method determines the cut-off frequency ν_0 from measurement and compares it to that from

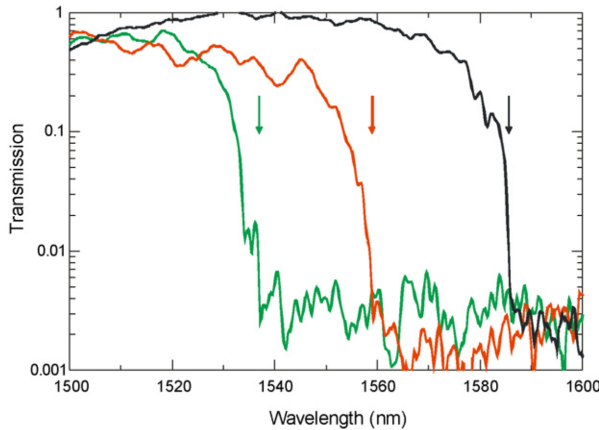

Fig. 3. (On-chip) transmission spectra of W1 membrane PhC waveguides (with design radius 284 nm) patterned at three different electron-beam doses, corresponding to dose factors 1.0 (black curve), 1.1 (red curve), and 1.2 (green curve). The cut-off wavelength of each waveguide is indicated by the arrows. (For interpretation of the references to color in this figure legend, the reader is referred to the web version of the article.)

calculation. However, we must first determine the error in the cut-off frequency $\Delta\nu_0$. This is related to the error in the reduced radius (i.e. $r' = r/a$) by the simple relationship

$$\Delta r' = \frac{\partial r'}{\partial \nu}\,\Delta\nu_0 \approx 4\,\Delta\nu_0, \tag{1}$$

where $\partial r'/\partial \nu$ is easily estimated from the calculations of Fig. 2, and has a value of 4 for $r' \approx 0.3$. The main sources of error are in the measurement of this cut-off and the uncertainty of the thickness of the silicon slab.

The thickness of the silicon slab is specified by the manufacturer of the SOI wafers (SOITEC) as $h \pm \Delta h = 220 \pm 5$ nm. Fig. 2 (inset) shows the calculated effect of altering this thickness on the value of the cut-off frequency obtained, and there is a clear linear relationship. This introduces an error $\Delta h\ \partial\nu_0/\partial h$, where $\partial\nu_0/\partial h$ is estimated from the slope of the line in Fig. 2 (inset). For the stated values, the estimated relative error in the hole diameter due to the uncertainty of the slab thickness is approximately 1.6%. This error represents the largest uncertainty in the method, and it could be reduced by measuring the thickness of the silicon in the particular wafer used, using (for example) ellipsometry. However, this measurement would need to be performed for every specific die used in the experiments, as h varies across the wafer, so it is not done in practice.

The error in the measurement of the cut-off wavelength ($\lambda_0 \pm \Delta\lambda_0$) is estimated from the transmission spectra, such as those shown in Fig. 3. Generally a value of $\Delta\lambda_0 = 2$ nm is obtained. This error is mainly due to the poor coupling of the slab waveguide mode to the slow-light mode of the W1 near cut-off [26,27], which complicates the identification of the actual cut-off wavelength λ_0. The error could be reduced by improving the coupling efficiency closer to the bandedge, using the design methods of [26] and [27], although this would significantly increase the design effort. Once λ_0 is measured, the reduced frequency of the cut-off is then $\nu_0 = a/\lambda_0$. We assume that the error in the lattice constant is negligible; thus the relative error in the reduced frequency of cut-off is around 0.1%.

It must also be noted that the measurement of the cut-off wavelength in transmission depends on the length of the W1 PhC waveguide. This is because the detector used in the experiments has a given sensitivity, and so the measurement of the cut-off will be slightly blue-shifted for longer waveguides that have higher losses. This effect adds a systematic bias to the measurement of the hole diameter (of around 0.5 nm) but can be minimised if the same length of waveguide is always used for reference, and if relatively short waveguides are used; these are 20 μm long in our case.

3. Results and discussion

Fig. 4 shows the key results: W1 PhC waveguides are fabricated on two separate chips (i.e. in two fabrication runs) with a range of electron-beam base doses. Each chip has W1s with holes of two distinct design

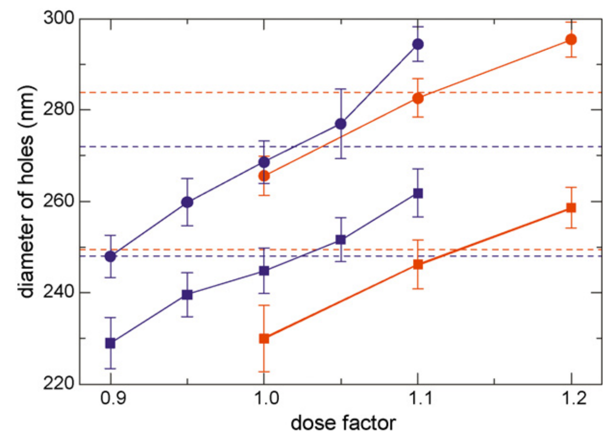

Fig. 4. Measurement of the diameter of holes in W1 PhC waveguides as a function of the electron-beam base dose for two fabrication runs (blue/red lines differentiate the two runs). The curves are coded as follows: blue squares, design diameter 248 nm; red squares, 250 nm; blue circles, 272 nm; and red circles, 284 nm. The horizontal dashed lines indicate the design diameter in each case. (For interpretation of the references to color in this figure legend, the reader is referred to the web version of the article.)

diameters. The first chip has design diameters of 250 nm (red squares in Fig. 4) and 284 nm (red circles); the second has design diameters of 248 nm (blue squares) and 272 nm (blue circles). For each waveguide the transmission spectrum was measured and the cut-off wavelength found; this was then compared to calculations. The error bars are estimated as per the discussion in the previous section. The errors do vary slightly, according to the estimated error on determining the cut-off wavelength, but the median error in the diameter is ±5 nm, or 2%.

For our process, the mean correct electron-beam dose is 52 ± 3 μAs/cm^2, and the dose factors in this paper refer to multiples of this. As they are from the same fabrication run, the two blues lines (and also the two red lines) in Fig. 4 should cross the design diameter for the same base dose—this is a measure of the correct electron-beam dose for that particular run. It can be seen that this is the case, and the correct dose in the two runs is given by dose factors of (just over) 1.0 and 1.1 respectively. Such a change in the correct dose between runs is normal; the 95% confidence interval is doses within 46–58 μAs/cm^2, a variation of up to 23%. The factors which cause such process variations are not well understood, but are probably related to the cleanroom environment when spinning the resist (for example, the humidity or temperature).

Fig. 4 also provides information on how the base dose affects the final hole size in the etched devices. A change of base dose by 1% alters the hole diameter by 2 nm. Referring back to the graph in Fig. 1(a), we can see that we must control the dose to better than 2% in order to control the hole size to ±4 nm and ensure the photonic crystal devices will operate in the 10 nm window indicated. Currently, this requires writing the same device patterns at base doses in increments of 2% over the 23% normal variation of the correct dose to get one working device. Post-processing steps to fine-tune the working wavelength, such as wet-chemical digital etching, deposition of nanometre oxide layers, or localised nano-oxidation [3–6], may also be required to achieve an exact working wavelength. This represents a large waste of electron-beam time and material resources, and for integrated devices consisting of two or more photonic crystal components, the problem is magnified, as all the components must work at the same wavelength as each other.

Current bench-mark repeatability for the hole diameter in successive photonic crystal fabrication runs is of the order of 5 nm [2]. As our optical measurement is capable of resolving these differences between runs, it enables a program of research into the factors in the fabrication process that cause this variability and how to reduce them. Such feedback loops will lead to improvements in the processing of photonic crystal slabs in order to improve the control and repeatability of the hole size between fabrication runs.

Acknowledgments

We would like to acknowledge the EU FP6-FET ‘‘Splash’’ project for funding and the Nanostructuring Platform of EU FP6-NoE ‘‘epixnet’’ for technical support.

References

[1] M. Settle, M. Salib, A. Michaeli, T.F. Krauss, Low loss silicon on insulator photonic crystal waveguides made by 193 nm optical lithography, Opt. Express 14 (6) (2006) 2440–2445.
[2] B.-S. Song, T. Nagashima, T. Asano, S. Noda, Resonant-wavelength control of nanocavities by nanometer-scaled adjustment of two-dimensional photonic crystal slab structures, Photonics Technol. Lett. 20 (7) (2008) 532–534.
[3] K. Hennessy, A. Badolato, A. Tamboli, P.M. Petroff, E. Hu, M. Atature, J. Dreiser, A. Imamoglu, Tuning photonic crystal nanocavity modes by wet chemical digital etching, Appl. Phys. Lett. 87 (2) (2005) 021108.
[4] K. Hennessy, C. Hogerle, E. Hu, A. Badolato, A. Imamoglu, Tuning photonic nanocavities by atomic force microscope nano-oxidation, Appl. Phys. Lett. 89 (4) (2006) 041118.
[5] X.D. Yang, C.J. Chen, C.A. Husko, C.W. Wong, Digital resonance tuning of high-Q/V-m silicon photonic crystal nanocavities by atomic layer deposition, Appl. Phys. Lett. 91 (16) (2007) 161114.
[6] E. Graugnard, D.P. Gaillot, S.N. Dunham, C.W. Neff, T. Yamashita, C.J. Summers, Photonic band tuning in two-dimensional photonic crystal slab waveguides by atomic layer deposition, Appl. Phys. Lett. 89 (18) (2006) 181108.
[7] R. Wuest, F. Robin, P. Strasser, H. Jackel, D. Erni, Influence of proximity effects in electron-beam lithography on the optical properties of planar photonic-crystal waveguides, J. Appl. Phys. 102 (2007) 083110.
[8] N. Yamamoto, T. Ogawa, K. Komori, Photonic crystal directional coupler switch with small switching length and wide bandwidth, Opt. Express 14 (3) (2006) 1223–1229.
[9] D.M. Beggs, T.P. White, L. O'Faolain, T.F. Krauss, Ultracompact and low-power optical switch based on silicon photonic crystals, Opt. Lett. 33 (2) (2008) 147–149.
[10] D. Mori, T. Baba, Wideband and low dispersion slow light by chirped photonic crystal coupled waveguide, Opt. Express 13 (23) (2005) 9398–9408.
[11] Yu. Petrov, M. Eich, Dispersion compensation with photonic crystal line-defect waveguides, IEEE J. Sel. Areas Commun. 23 (7) (2006) 1396–1401.
[12] J. Smajic, C. Hafner, D. Erni, Design and optimization of an achromatic photonic crystal bend, Opt. Express 11 (12) (2003) 1378–1384.

[13] S. Assefa, S.J. McNab, Y.A. Vlasov, Transmission of slow light through photonic crystal waveguide bends, Opt. Lett. 31 (6) (2006) 745–747.

[14] C. Jin, N.P. Johnson, H.M.H. Chong, A.S. Jugessur, S. Day, D. Gallagher, R.M. De La Rue, Transmission of photonic crystal coupled resonator waveguide (PhCCRW) structure enhanced via mode matching, Opt. Express 13 (7) (2005) 2295–2302.

[15] S. Noda, A. Chutinan, M. Imada, Trapping and emission of photons by a single defect in a photonic bandgap structure, Nature 407 (6804) (2000) 608–610.

[16] L.H. Frandsen, A.V. Lavrinkenko, J. Fage-Pedersen, P.I. Borel, Photonic crystal waveguides with semi-slow light and tailored dispersion properties, Opt. Express 14 (20) (2006) 9444–9450.

[17] T.F. Krauss, B. Vogele, C.R. Stanley, R.M. DelaRue, Waveguide microcavity based on photonic microstructures, Photonics Technol. Lett. 9 (2) (1997) 176–178.

[18] A. Chutinan, S. Noda, Waveguides and waveguide bends in two-dimensional photonic crystal slabs, Phys. Rev. B 62 (7) (2000) 4488–4492.

[19] M. Notomi, K. Yamada, A. Shinya, J. Takahashi, C. Takahashi, I. Yokohama, Extremely large group-velocity dispersion of line-defect waveguides in photonic crystal slabs, Phys. Rev. Lett. 87 (25) (2001) 253902.

[20] S.J. McNab, N. Moll, Y.A. Vlasov, Ultra-low loss photonic integrated circuit with membrane-type photonic crystal waveguides, Opt. Express 11 (22) (2003) 2927–2939.

[21] T.F. Krauss, Photonic crystals shine on, Phys. World 19 (2) (2006) 32–36.

[22] K.M. Ho, C.T. Chan, C.M. Soukoulis, Existence of a photonic gap in periodic dielectric structures, Phys. Rev. Lett. 65 (1990) 3152–3155.

[23] S.G. Johnson, J.D. Joannopoulos, Block-iterative frequency domain methods for Maxwell's equations in a planewave basis, Opt. Express 8 (3) (2000) 173–190.

[24] J.A. McCaulley, V.M. Donnelly, M. Vernon, I. Taha, Temperature dependence of the near-infrared refractive index of silicon, gallium arsenide, and indium phosphide, Phys. Rev. B 49 (11) (1994) 7408–7417.

[25] L. O'Faolain, X. Yuan, D. McIntyre, S. Thoms, H. Chong, R.M. De la Rue, T.F. Krauss, Low-loss propagation in photonic crystal waveguides, Electron. Lett. 42 (25) (2006) 1454–1455.

[26] Y.A. Vlasov, S.J. McNab, Coupling into the slow light mode in slab-type photonic crystal waveguides, Opt. Lett. 31 (1) (2006) 50–52.

[27] J.P. Hugonin, P. Lalanne, T.P. White, T.F. Krauss, Coupling into slow-mode photonic crystal waveguides, Opt. Lett. 32 (18) (2007) 2638–2640.